Neutron Diffraction Studies on the Location of Water in Lecithin Bilayer Model Membranes

(membrane structure/bound water/H₂O–D₂O exchange/phospholipid bilayer)

G. ZACCAI*‡, J. K. BLASIE†, AND B. P. SCHOENBORN*

* Biology Department, Brookhaven National Laboratory, Upton, New York 11973; and † Department of Biophysics and Physical Biochemistry, Johnson Research Foundation, University of Pennsylvania, Philadelphia, Pa. 19174

ABSTRACT Lamellar neutron diffraction from oriented multilayers of hydrated dipalmitoyl lecithin was phased by isomorphous H₂O–D₂O exchange and swelling techniques. Bound water sites were located in the polar head group region of the bilayer profile. A 6-Å resolution structure based on the neutron scattering density profile is proposed for the bilayer. It is consistent with the electron density profile from x-ray diffraction.

Because of their ubiquitous presence in biological membranes, phospholipids have been studied extensively. They are amphipathic in character and have interesting and varied physical properties when combined with water (1–8). Differential scanning calorimetry measurements showed that dipalmitoyl lecithin can bind up to 20% of its weight in water (2), and Chapman has suggested that this bound water might be indispensible to membrane structure and function. While x-ray diffraction has provided considerable insight into molecular organization in natural and model membranes, its use in the location of bound water is, at best, indirect because of the weak x-ray scattering of water (5–7). It is, however, possible to locate water molecules directly by neutron diffraction (9). Neutrons interact with atomic nuclei rather than electron clouds as in the case of x rays, and neutron scattering lengths are of the same order of magnitude for all elements, including hydrogen (10). Different isotopes, however, may have different scattering lengths and in particular the values for hydrogen and deuterium are −3.7 and +6.7 Fermi units, respectively. This is a relatively large difference (11), which can be used for differential labeling similar to the heavy atom techniques of x-ray structure analysis (12), with the additional advantage that H–D exchange allows true isomorphism, as has been shown in a number of systems by x-ray diffraction.

Phospholipid–water systems can form oriented multilayers which consist of alternate sheets of bimolecular lipid layers and water (3, 5–7). In this paper we describe the analysis of lamellar neutron diffraction from such multilayers of dipalmitoyl lecithin (DPL). H₂O–D₂O exchange in the multilayers allowed not only locating of the bound water but also the phasing of the neutron profile structure (the projection of neutron scattering density onto a line normal to the multilayer surface) by conventional Patterson function techniques. This phase determination was further verified by the swelling method, a technique that has been used to phase lamellar x-ray diffraction from membranes (3, 6, 13).

Abbreviation: DPL, dipalmitoyl lecithin.

‡ Present address: Institut Laue-Langevin, B.P. 156 Centre de Tri, 38042 Grenoble Cedex, France.

We understand that somewhat similar studies have been in progress at A.E.R.E., Harwell, U.K. (D. Worcester, M. Wilkins, and B. T. M. Willis, personal communication).

MATERIALS AND METHODS

Samples were prepared by allowing sonicated dispersions of DPL (from Calbiochem) in H₂O buffer (1 mM potassium phosphate, pH 7.5) to dry by slow evaporation (3–5 hr) on glass slides 6 × 2.5 cm². Typically, a sample contained 50 mg of DPL. The molecular ratios of lecithin to buffer were close to 30:1. In the H₂O–D₂O exchange, the sample was rewet with D₂O and allowed to dry in a very low humidity D₂O atmosphere. This was repeated four times to ensure maximum exchange.

Data were collected at the High Flux Beam Reactor using the Brookhaven low angle diffractometer operating at 4.2 Å (11). Incident beam width was adjusted via slit collimation to match the sample projection, which varied with each lamellar reflection. For the low order reflections ($h = 1–4$), however, the beam width was maintained at 1 cm to allow the full divergence of the beam to impinge on the sample.

Lamellar intensity data were collected by scanning both the sample and the detector ($\theta–2\theta$ scans), counting times varying according to the strength of each reflection. The first four orders were relatively strong and could all be collected in a day. Higher orders had to be scanned repeatedly and averaged. For these scans it was especially important to maintain constant temperature and relative humidity, as some of the intensities varied greatly with the periodicity of the multilayers. Since at a steep portion of the continuous unit cell transform there could be large changes in intensity for changes in d that are too small to measure, a test for the reproducibility of the data is whether the Fourier syntheses yield identical profiles at the same resolution. By this criterion, data collected over several months from different DPL samples were reproducible.

The mosaic spread η was measured by rotating the sample with the detector stationary at the correct 2θ for each reflection (ω scans). Two such scans are shown in Fig. 1. The minima in intensity were due to high absorption where the plane of the sample was parallel to the incident beam or where it was parallel to the diffracted beam. Values of η varied between 20 and 30°. The ω scans also showed that the intensities at 15% relative humidity had to be corrected by a factor of 3 for $I(1)$, while $I(2)$ and $I(3)$ had to be corrected by 1.6 and 1.4, respectively. (Fig. 1).

The appropriate Lorentz correction for each reflection $I(h)$ was h^2, where h is the order number. One factor of h is the

usual one for lamellar reflections (15) (the Lorentz correction $\sin 2\theta$ is proportional to h for small θ; for the higher order reflections it is a good approximation because of the large standard deviation of the intensities); the other factor of h arose from the fact that the reflections were smeared vertically by the mosaic spread ($\eta \simeq 25°$) and the incident beam divergence into arcs higher than 2 cm (the slit height at the detector). This was later confirmed with a two-dimensional position-sensitive detector (14) which clearly showed the vertical extent of the reflections and their shape. Thus the structure factor moduli were related to the intensities by

$$|F(h)| = (h^2 I(h))^{1/2}$$

RESULTS

In a one-dimensional centrosymmetric profile, the neutron scattering density is given by

$$\rho(x) = \sum_h \epsilon(h)|F(h)|\cos 2\pi hx/d. \qquad [1]$$

The units of $\rho(x)$ are $b/Å^3$ where b is the relative neutron scattering length. For the bilayers, x is length along a line normal to their surface, d is the unit cell repeat distance; the phase factors $\epsilon(h)$ are either $+1$ or -1 and have to be determined. There are centers of symmetry at $x = 0$ and $\pm d/2$.

Lamellar neutron intensity data were collected from DPL–H$_2$O and DPL–D$_2$O oriented multilayer samples at 20°C and 15% relative humidity and for DPL–H$_2$O alone at 20°C and 35% relative himidity (Table 1).

Low resolution reflections ($h = 1$–4) of DPL–H$_2$O and DPL–D$_2$O were phased by the isomorphous replacement method. The high resolution reflections ($h = 5$–10), for which the standard deviations were considerably larger (Table 1), were phased by both isomorphous replacement and swelling methods. In the following paragraphs we first describe the isomorphous replacement method and then the swelling analysis used.

The structural contributions to $\rho(x)$ can be separated and we can write for the profile projection of DPL–H$_2$O:

$$\rho(x) = \sum_k \rho_k(x) + \rho_{H_2O}(x) \qquad [2]$$

where k is over all atoms excepting the atoms in the H$_2$O molecules. In the DPL–D$_2$O unit cell:

$$\rho'(x) = \sum_k \rho_k(x) + \rho_{D_2O}(x) \qquad [3]$$

$$\rho'(x) - \rho(x) = \rho_{D_2O}(x) - \rho_{H_2O}(x). \qquad [4]$$

Using Eq. 1 and writing $\Delta\rho(x) = \rho'(x) - \rho(x)$:

$$\Delta\rho(x) = \sum_h \{F_{D_2O}(h) - F_{H_2O}(h)\} \cos 2\pi hx/d \qquad [5]$$

where $F_{D_2O}(h)$ and $F_{H_2O}(h)$ are correctly phased. From Eq. 4 it is seen that $\Delta\rho(x)$ is zero at all x values except where H has been replaced by D. Since there are no exchangeable H atoms in lecithin, $\Delta\rho(x)$ is identical with the distribution of water in the structure with each molecule having a scattering length equal to $b_{D_2O} - b_{H_2O}$.

The difference Patterson is given by

$$\Delta P(x) = \sum_h [F_{D_2O}(h) - F_{H_2O}(h)]^2 \cos 2\pi hx/d. \qquad [6]$$

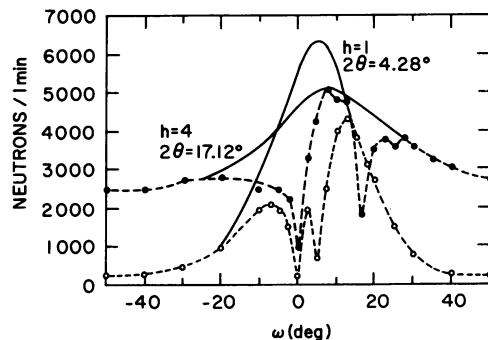At low water contents, it can be shown that strong reflections

FIG. 1. ω Scans of the first and fourth order lamellar reflections of DPL–H$_2$O at 15% relative humidity. The broken lines are the loci of measured intensities. The solid lines are the Gaussian envelopes peaking at $\omega = 0$. The observed intensity minima occur when the plane of the sample is either parallel to the incident or the diffracted beam. The $h = 4$ reflection need not be corrected for absorption because the ω scan has a plateau in the vicinity of 8.5°; it shows, however, that intensities at $\omega = 2°$ are depressed by a factor of 3. $I(1)$ at $\theta \sim 2°$ should, therefore, be corrected by $\times 3$ [see footnote (†) to Table 1]. This value accounts well for the difference between the observed intensity at $\omega = 2°$ and the Gaussian envelope for $h = 1$. Intensity scale factor $k = 1/30$ for $h = 4(\bullet)$ and $k = 1$ for $h = 1(\bigcirc)$.

from the hydrated multilayer are not expected to change sign as a result of the exchange and it is a good approximation to write for the low resolution difference Patterson:

$$\Delta P(x) = \sum_{h=1}^4 [|F_{D_2O}(h)| - |F_{H_2O}(h)|]^2 \cos 2\pi hx/d.$$

Such a low resolution difference Patterson with or without a change in sign of the weak second order reflection due to the

TABLE 1. *Structure factors**

h	$d = 56.0 \pm 0.5$ Å (15% relative humidity)		$d' = 59.0 \pm 0.5$ Å (35% relative humidity)
	DPL–D$_2$O $F(h)$	DPL–H$_2$O $F(h)$	DPL–H$_2$O $F_0(n)$
1†	317 ± 15	190 ± 11	180 ± 9
2	49 ± 3	20 ± 4	29 ± 2
3	43 ± 3	77 ± 4	97 ± 5
4	67 ± 2	85 ± 6	74 ± 2
5	0 ± 5	0 ± 6	Not measured
6	23 ± 6	40 ± 5	26 ± 3
7	26 ± 5	48 ± 7	0 ± 3
8	47 ± 5	43 ± 9	40 ± 4
9	48 ± 8	52 ± 12	26 ± 10
10	31 ± 13	57 ± 11	0 ± 10

* $F(h) = (h^2 I(h))^{1/2}$; $\sigma(I) = \sqrt{(\text{total intensity}) + (\text{background})}$; $\sigma(F)/F = \sigma(I)/2I$.

† $I(1)$, $I(2)$, and $I(3)$ values have been corrected for absorption empirically from the ω scan of $I(4)$ (Fig. 1). The corrections at 15% relative humidity are 3.0 for $I(1)$, 1.6 for $I(2)$, and 1.4 for $I(3)$. At 35% relative humidity they are 3.5 for $I(1)$, 1.9 for $I(2)$, and 1.5 for $I(3)$. The indicated errors include the uncertainty in the absorption correction and slit smearing. The effects of these errors are minimized in the difference syntheses since both the H$_2$O and the D$_2$O DPL data sets were collected from the same sample.
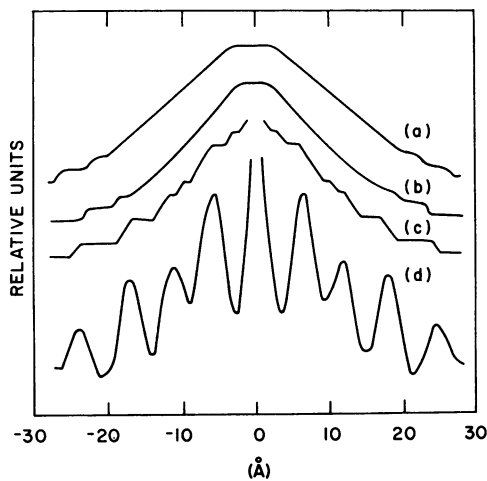
FIG. 2. Difference Pattersons: (a) Low resolution map for first four orders. No changes in sign between H_2O and D_2O samples. (b) Same as (a) except that the weak second order changed sign. (c) High resolution map for the first 10 orders, only the second order changed sign. (d) Final difference Patterson where $h = 2, 6, 7, 9, 10$ changed sign between the H_2O and D_2O samples.

H_2O–D_2O exchange is consistent with $\Delta\rho(x)$ represented by a rectangular strip of width $w_\Delta = 10$ Å at a center of symmetry (Fig. 2a and b). This provides a site for the isomorphous replacement at this resolution. These parameters were used to determine the phases ϵ ($h = 1$–4) by adapting Hargreaves' method for centrosymmetric structures (12). The structure factors are given by:

$$aF_{H_2O}(h) = \frac{2}{\pi h}\,\rho_H \cos\frac{2\pi h x_\Delta}{d}\,\sin\frac{\pi h w_\Delta}{d}$$
$$+ \sum_{k\neq\Delta}\frac{2}{\pi h}\,\rho_k \cos\frac{2\pi h x_k}{d}\,\sin\frac{\pi h w_k}{d} \quad [7]$$

$$bF_{D_2O}(h) = \frac{2}{\pi h}\,\rho_D \cos\frac{2\pi h x_\Delta}{d}\,\sin\frac{\pi h w_\Delta}{d}$$
$$+ \sum_{k\neq\Delta}\frac{2}{\pi h}\,\rho_k \cos\frac{2\pi h x_k}{d}\,\sin\frac{\pi h w_k}{d} \quad [8]$$

where subscript Δ is for the strip contributed by the water, a and b are scale factors. Subtracting and rearranging yields

$$\frac{aF_{H_2O}(h)}{\dfrac{1}{h}\cos\dfrac{2\pi h x_\Delta}{d}\,\sin\dfrac{\pi h w_\Delta}{d}} - \frac{bF_{D_2O}(h)}{\dfrac{1}{h}\cos\dfrac{2\pi h x_\Delta}{d}\,\sin\dfrac{\pi h w_\Delta}{d}}$$

$$+ \frac{2}{\pi}(\rho_D - \rho_H) = 0 \quad [9]$$

where a and b are equal when the same sample is used for the H_2O and D_2O data collection. Plotting $A(h)$ against $B(h)$, where $A(h) = F_{D_2O}(h)\left(\dfrac{1}{h}\cos\dfrac{2\pi h x_\Delta}{d}\,\sin\dfrac{\pi h w_\Delta}{d}\right)$ and $B(h)$ $= F_{H_2O}(h)\left(\dfrac{1}{h}\cos\dfrac{2\pi h x_\Delta}{d}\,\sin\dfrac{\pi h w_\Delta}{d}\right)$, would, therefore, yield a straight line of slope 1 if $F_{H_2O}(h)$ and $F_{D_2O}(h)$ are correctly phased (Fig. 3). The phases thereby found for $F_{D_2O}(h)$ were $+1+1-1-1$ and for $F_{H_2O}(h)$ they were $+1-1-1-1$. Changing the signs of the odd orders shifts the origin to the
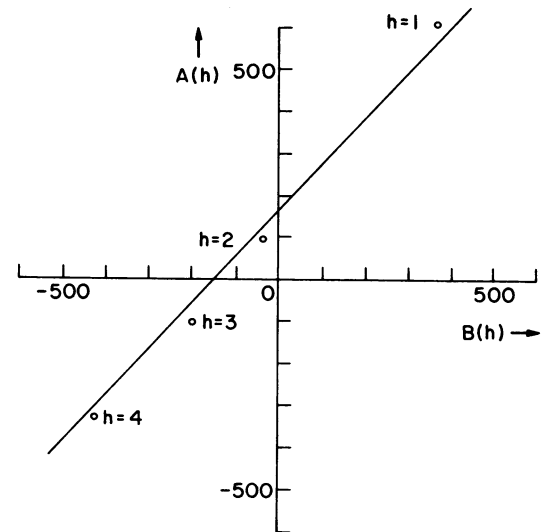

FIG. 3. Hargreaves' plot for the first four orders of DPL–D_2O and DPL–H_2O.

other center of symmetry for consistency with previously published x-ray scattering density profiles. Note that in the new frame of reference the water is located around $x = \pm d/2$ Å. The low resolution profiles of DPL–H_2O, DPL–D_2O, and their difference are shown in Fig. 4a–c.

The higher order reflections ($h = 5$–10) were weaker and had larger standard deviations than the lower orders (Table 1). In general a number of reflections could have changed sign as a result of the exchange. It was, therefore, uncertain whether for each reflection h,

$$|\Delta F(h)| = |F_{D_2O}(h)| - |F_{H_2O}(h)| \text{ or}$$
$$|\Delta F(h)| = |F_{D_2O}(h)| + |F_{D_2O}(h)|.$$

As a first approximation $\Delta P(x)$ was calculated assuming no sign changes for reflections $h = 5$–10. $\Delta P(x)$ in the region $-d/2 < x < + d/2$ was then deconvoluted to yield the first approximation to the 6-Å resolution water distribution $\Delta\rho(x)$, since the low resolution difference Patterson showed that water was predominately located within ±5 Å of $x = d/2$ Å. An additional criterion for $\Delta\rho(x)$ was obtained from the low resolution structure (Fig. 4c), which shows that the water distribution is flat and zero in the center of the bilayer. Small fluctuations in $\Delta\rho(x)$ around $x = 0$ Å at high resolution would then be due to noise arising from errors in the structure factors and from series termination effects. Therefore, a rectangular strip model which was flat around $x = 0$ was calculated for $\Delta\rho(x)$ from the deconvolution of ΔP ($-d/2 < x < + d/2$). Structure factors were calculated for the model and each compared to the two possible values for the observed $|\Delta F(h)|$. A difference Patterson was then calculated using the observed $|\Delta F(h)|$ that best agreed with the model. The procedure was repeated cyclically until there was agreement within errors between observed and calculated structure factors. Fig. 2c and d shows the first approximation to $\Delta P(x)$ and the final (best) $\Delta P(x)$ for which orders $h = 2, 6, 7, 9, 10$ were required to change sign on H_2O–D_2O exchange. The resulting 6-Å resolution structures are depicted in Fig. 4d–g together with the effect of errors on $\Delta\rho(x)$.

This iterative isomorphous replacement approach using the difference Patterson would be an exact method if changes in

$\epsilon(h)$ on H_2O–D_2O exchange either did not occur or were known. Such procedures beginning with a structure in H_2O or D_2O followed by partial H_2O–D_2O exchange so that $\epsilon(h)$ values do not change even for higher orders have recently been used by us to phase lecithin–cholesterol bilayer profiles. The second alternative, i.e., observing phase changes on exchange, has become accessible with the use of a position-sensitive detector (14). The rate of D_2O–H_2O exchange in hydrated bilayers was observed to be of the order of several minutes.

Because of the large standard deviations of the higher order intensities and resulting possible correlations between their different phase combinations in the iterative isomorphous replacement procedure, reflections $h = 5$–10 of DPL–H_2O were also phased by the swelling method. The unit cell dimension was swollen by 5% by increasing the relative humidity to 35%. The Fourier sampling theorem (6, 16) combined with variance analysis was then used to find that set of phases for the lower humidity reflections ($h = 5$–10) that best predicted the intensities observed at the higher humidity. The phases of $h = 1$–4 were maintained constant as determined by the isomorphous replacement procedure. The assumption is made in the swelling method that the unit cell increases because of a slightly wider water layer between lipid bilayers, while the structure of the bilayers remains unchanged. The diffracted amplitudes then fall on an essentially constant transform; consequently, changing the periodicity merely changes the sampling interval. The Fourier sampling theorem states that

$$\epsilon(n/d')|F(n/d')| = \sum_{-h_{max}}^{+h_{max}} \epsilon(h/d)|F(h/d)| \frac{\sin \pi(nd/d' - h)}{\pi(nd/d' - h)} \quad [10]$$

where $\epsilon(n/d')$ and $F(n/d')$ are the nth order phase and structure factors, respectively, of the swelled structure with unit cell d'.

It has been shown that, assuming no change in the bilayer structure, increasing the water content decreases the resolution to which it can be determined (6, 7). Whether this arises from increased static disorder or dynamic effects within the multilayer lattice is unclear. As a first approximation it can be accounted for by writing

$$F_c(n/d') = F(n/d') \exp(-Bn^2/4d'^2) \quad [11]$$

where B is analogous to a Debye–Waller factor due to simple lattice disorder caused by increased water content between 15% and 35% relative humidity.

The observed structure factors at 35% relative humidity, $|F_0(n/d')|$, are shown in Table 1. Since the same sample was used for both the higher and the lower relative humidity experiments, it was assumed that no scale factor was involved in the comparison of $F_0^2(n/d')$ and $F_c^2(n/d')$. Two parameters could not be measured, $F(0/d)$ and B. $F(0/d)$ is a constant which sets the scattering density of the water between lipid bilayers to zero. It was estimated from the values at $\pm d/2$ in the low resolution profile (Fig. 4a and c) to be 75 ± 25 in the same units as $F(h/d)$. A first estimate of B was made by comparing the $F_c^2(n/d')$ and $F_0^2(n/d')$ for $n = 1$–4, since the phases of these reflections were known. B was then varied to gauge its effect on $F_c^2(n/d')$ ($n = 1$–10). It was found that $F_0^2(n/d') - F_c^2(n/d')$ were not very sensitive to variations of B within the limits $B = 50 \pm 7$ Å^2.

The best agreement between a set of $F_c^2(n/d')$ and $F_0^2(n/d')$ was found by examining the difference $D(n/d')$ and its standard deviation $\sigma(n/d')$.
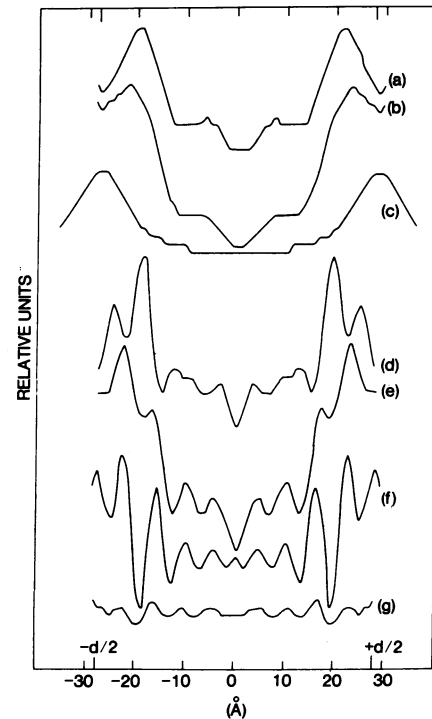

FIG. 4. The bilayer profiles at 15-Å resolution ($h = 1$–4). (a) DPL–H_2O, phases $-1,-1,+1,-1$; (b) DPL–D_2O, phases $-1,+1,+1,-1$; (c) the difference which is equivalent to the water distribution. The bilayer profiles at 6-Å resolution ($h = 1$–10); all are on the same scale. (d) DPL–H_2O phases $-1,-1,+1,-1,0,+1,-1,-1,+1,-1$; (e) DPL–$D_2O$ phases $-1,+1,+1,-1,0,-1,+1,-1,-1,+1$; (f) the water distribution $\Delta\rho(x)$; (g) Fourier synthesis using the standard deviations of $\Delta F(h)$ as coefficients with the phases of $\Delta F(h)$. It shows the effect of errors on $\Delta\rho(x)$.

$$D(n/d') = |F_0^2(n/d') - F_c^2(n/d')| \quad [12]$$

$$\sigma(n/d') = \{var[F_0^2(n/d')] + var[F_c^2(n/d')]\}^{1/2}. \quad [13]$$

The $var[F_c^2(n/d')]$ values were calculated from

$$var[F_c(n/d')] = \sum_{-h_{max}}^{+h_{max}} var[F(h/d)] \frac{\sin^2 \pi(nd/d' - h)}{\pi^2(nd/d' - h)}. \quad [14]$$

The relative probability $\phi(D)$ of obtaining a value of $D(n/d')$, assuming a normal distribution, is:

$$\phi(D) = \frac{1}{\sigma\sqrt{2\pi}} \exp\left(\frac{-D^2}{2\sigma^2}\right) \quad [15]$$

Each set of phases $\epsilon(h)$ corresponds to a set of $D(n/d')$ with a joint relative probability J

$$J = \prod_n \phi[D(n/d')] \quad [16]$$

A larger value of J indicates a better fit between observed and calculated values.

This approach yielded three sets of phases which consistently gave larger values of J (a factor of approximately 10 better than other phase sets). Of these three sets, one is identical to that obtained above by isomorphous replacement (Fig. 4e). The agreement between the two independent phasing procedures is taken to establish the phases of DPL–H_2O.

Furthermore, the other two profiles yielded by the swelling method are inconsistent with the isomorphous replacement

phasing. They have local maxima at the center of the bilayer so that a molecular interpretation of those profiles would not only be incompatible with the 15-Å low resolution profile of Fig. 4b but also chemically awkward to interpret.

In summary, therefore, a comparison of the isomorphous replacement and swelling procedures yielded the 6-Å resolution neutron scattering density profile of the DPL–H$_2$O bilayer. The distribution of water sites in the bilayer was obtained by isomorphous H$_2$O–D$_2$O exchange. Three water sites appeared in the bilayer profile at 16 Å, 23 Å, and at the cell edge (Fig. 4f).

DISCUSSION

The molecular interpretation of the neutron scattering density profile of DPL–H$_2$O at low water content is in good agreement with a model based on x-ray results (5, 6). The neutron and x-ray scattering profiles were determined independently and neutron and x-ray scattering lengths are quite different. There is, therefore, good evidence for this molecular model. Furthermore, the neutron experiment directly yielded bound water locations that previously could only be inferred.

At 15-Å resolution (Fig. 4), the peaks at $x = \pm 20$ Å correspond to the lecithin polar head groups, and the trough at $x = 0$ Å to the terminal methyl groups of the alkyl chains with the portion of constant density in between corresponding to the chains themselves. We estimated that the scattering density in the water distribution was equivalent to 3 ± 1 molecules of water per lipid molecule. The water appears predominantly around the head groups, but even at low resolution it is clear from the shoulder at $x = \pm 15$ Å (Fig. 4c) that it penetrates right up to the level of the hydrocarbon chains.

A simple indication of the relative scattering density distribution at higher resolution (Fig. 4e) was obtained by fitting a rectangular strip model to the observed DPL profile. The observed profile was reproduced within its errors by calculating a profile of the DPL bimolecular leaflet based on a rectangular strip model with the chains' terminal methyl groups occupying 4 Å at the center, the glycerol moieties in 4.5 Å at $x = \pm 19.5$ Å, the choline phosphate moieties in 4.5 Å at $x = \pm 25$ Å, and the alkyl chains occupying approximately 15 Å along $\pm x$. All the groups are assumed to occupy the same cross sectional area perpendicular to x.

At 6-Å resolution the water sites are at the cell edge, at $x = 23$ Å and $x = 16$ Å. On the molecular model these correspond to 1.5 ± 0.3 molecules of water between polar head groups of adjacent bilayers, 1.3 ± 0.3 molecules overlapping the choline phosphate and glycerol moieties and 0.7 ± 0.2 molecules on the glycerol edge adjacent to the alkyl chains. It was pointed out from x-ray experiments (5–7) that the electron density profile could also be interpreted as described above but with two water molecules assumed to be within each of the glycerol moieties in the head groups. This is consistent with the neutron results if the water site at 23 Å is considered as predominantly overlapping the glycerol moiety rather than the choline phosphate.

The projection of a carbon–carbon bond onto the axis of all *trans* alkyl chains is 1.25 Å; for the chains to fit in the 15 Å flat portion they would have to be tilted relative to the bilayer normal by 31°, yielding a "phase" for the oriented multilayers similar to the one labeled Lβ by Tardieu *et al.* (8). However, because of the uncertainty in the precise location of the chains' carbonyl groups within the 4.5-Å region containing the glycerol moiety, the degree of tilt is uncertain. Tilted chains are, however, inconsistent with the equatorial nature of the x-ray diffraction which arises from the chain packing in the plane of the bilayer under these conditions (7).

Finally, we must emphasize the conditions of the experiment. It was performed at 20°C with samples of relatively low water content (approximately 10%). The alkyl chains were in the frozen state. It would be of great interest to study both head group conformation and bound water sites at higher water content and above the chains' phase transition. We suspect, however, that this would be a difficult experiment, as the increased lattice disorder in these conditions may tend to limit resolution.

1. Luzzati, V. (1968) in *Biological Membranes*, ed. Chapman, D. (Academic Press, London), pp. 71–123.
2. Chapman, D. & Wallach, D. (1968) in *Biological Membranes*, ed. Chapman, D. (Academic Press, London), pp. 125–202.
3. Levine, Y. K. & Wilkins, M. H. F. (1971) *Nature New Biol.* **230,** 69–72.
4. Wilkins, M. H. F., Blaurock, A. E. & Engelman, D. M. (1971) *Nature New Biol.* **230,** 72–76.
5. Wilkins, M. H. F. (1971) *Ann. N.Y. Acad. Sci.* **195,** 291–292.
6. Lesslauer, W., Cain, J. E. & Blasie, J. K. (1972) *Proc. Nat. Acad. Sci. USA* **69,** 1499–1503.
7. Cain, J., Santillan, G. & Blasie, J. K. (1972) in *Membrane Research*, ed. Fox, C. F. (Academic Press, Inc., New York), pp. 3–14.
8. Tardieu, A., Luzzati, V. & Reman, F. C. (1973) *J. Mol. Biol.* **75,** 711–733.
9. Schoenborn, B. P., Nunes, A. C. & Nathans, R. (1970) *Ber. Bunsenges. Phys. Chem.* **74,** 1202–1207.
10. Bacon, G. E. (1972) *Neutron Diffraction* (Clarendon Press, Oxford).
11. Schoenborn, B. P. & Nunes, A. C. (1972) *Annu. Rev. Biophys. Bioeng.* **1,** 529–552.
12. Stout, G. & Jensen, L. (1968) in *X-Ray Structure Determination* (Macmillan, New York), pp. 267–300.
13. Moody, M. F. (1963) *Science* **142,** 1173–1174.
14. Alberi, J., Fischer, J., Radeka, V., Rogers, L. C. & Schoenborn, B. P. (1974) *Trans. IEEE, Nuclear Science,* in press.
15. *International Tables for X-ray Crystallography* (1959) (The Kynoch Press, England), Vol. 2, p. 266.
16. Sayre, D. (1954) *Acta Crystallogr.* **5,** 264.